Aalborg Universitet

AALBORG UNIVERSITY

Stochastic control of wave energy converters with constrained displacements for optimal power absorption

Sun, Tao; Nielsen, Søren R. K.; Basu, Biswajit

Stochastic control of wave energy converters with constrained displacements for optimal power absorption

Tao Sun [a,] [*], Søren R.K. Nielsen [a], Biswajit Basu [b]

[a] *Department of Civil Engineering, Aalborg University, 9000 Aalborg, Denmark*
[b] *Department of Civil, Structural and Environmental Engineering, Trinity College Dublin, Dublin 2, Ireland*

ABSTRACT

An semi-analytical solution is derived for the optimal control of the power take-off of a single-degree of freedom heave point absorber with constraints on the displacement. At first the control force is derived during states, where the displacement constraint is active. This results in an open-loop control law dependent on the external wave load on the absorber. Next, the analytical solution for the optimal control in the unconstrained state is indicated, which turns out to be of the closed loop type with feedback from the present displacement and acceleration and from future velocities. The derived control law contains an undetermined constant, which is calibrated at the interface to the previous constrained state. The approach requires the estimation of the wave load during the constrained states, and the prediction of the future velocity response during unconstrained states. An algorithm has been devised in the paper for handling these problems. The theory has been validated against numerical solutions obtained by nonlinear programming.

1. Introduction

A wave energy point absorber has horizontal dimensions significantly smaller than the dominating wave length. Especially, a heave point absorber is constrained by a mooring system or otherwise to enforce a motion merely in the vertical direction, and hence can be modeled as a single-degree-of-freedom oscillator.

In reality constraints are present on the displacement of the absorber, because the actuator has a limited stroke. Displacement constraints may also be imposed to prevent the absorber from hitting the sea-bottom or jumping out of the water, which may lead to damaging impact loadings on the outer shell of the absorber. Similarly, constraints are present on the control force due to saturation in the actuator system.

In this paper only displacement constraints of the absorber is considered. Displacement constraints are difficult to deal with since the constraint does not depend explicitly on the control force and the state variables can only be controlled indirectly through the equation of the motion of the system. Hartl et al. [1] presented a survey of maximum principles for optimal control problems with state constraints. In the so-called the direct adjoining approach, also known as the penalty function method [2], the state constraints are introduced into the Hamiltonian via adding Lagrange multipliers. The indirect adjoining approach, also known as the slack variable method, is based on the differentia-

tion of the state constraints which explicitly depends on the control force and is adjoined to the Hamiltonian. Jacobson and Lee [3] transformed an optimal control problem with a state inequality constraint into an unconstrained problem of higher dimension by slack variable method where the slack variable becomes the new control variable. The necessary conditions of optimality is presented based on Pontryagin's maximum principle and is solved by conjugate gradient method [4]. However, numerical difficulties may occur due to the increase dimension of the state vector. Eidsmoen [5] utilized an end-stop device modeled by a friction force to restrict the oscillating amplitude for a floating wave energy converter and determined an optimal control strategy based on variations of a Lagrange functional, subsequently solved by numerical method. Further, the unconstrained case and constrained case in regular an irregular sea-states are compared. Perez and Garcia [6] presented a state constrained optimal control strategy applied for monitoring supervisory control in hybrid electric vehicles. The solution with constraints on both the control force and state vector is derived based on Pontryagin's maximum principle. However, it is difficult to use the method straightforwardly, since the future instants of time at which these switching occur are unknown. Further, the co-state vector is also unknown. Instead, a nonlinear programming approached based on projected augmented Lagrangian algorithm was used to solve this constrained optimization problem. This is only applicable if the external loading is known throughout the control horizon. Hals et al. [7] studied optimal constrained motion of wave-energy converters based on a heaving, semi-submerged sphere. They formu-
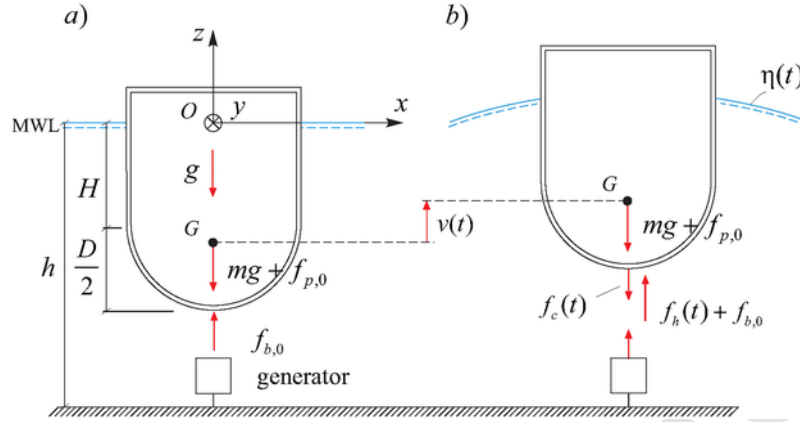
Fig. 1. Loads on heave absorber. (a) Static equilibrium state. (b) Dynamic state.

Table 1
Heave absorber and wave excitation parameters.

Parameter	Value	Unit	Parameter	Value	Unit
H	7.00	m	m_h	0.44×10^6	kg
D	14.00	m	k	1.51×10^6	N/m
h	30.00	m	H_s	3.00	m
m	1.84×10^6	kg	T_p	7.42	s

lated the dynamic programming problem with the maximum absorbed power considering the constraints on the heave excursion and the machinery force. Again, the future wave loading is required. It shows how amplitude constraint affects the amount of absorbed power. Sichani et al. [8] studied the optimal control law of a non-linear wave energy point absorber under the displacement and the control force constraints. Further, the displacement constraints were considered in terms of increasing control stiffness as the absorber approaches the boundary. Wang et al. [9] investigated the optimal control of a WEC with the constrained PTO force and the constrained motions of the converter in term of truncated Fourier series in time domain, where the problem is converted to a optimization problem with a convex quadratic objective functional and nonlinear constraints.

The present paper presents a semi-analytical solution for the optimal control of a heave point absorber with constraints on the displacement. The suggested solution is optimal between the intervals, where the displacement constraints are not active. During the intervals with active displacement constraints, an approximate feedforward control is applied. Because the time intervals with active constraints diminish as the level of the constraints is increased, the suggested solution will approach the optimal solution asymptotically at high displacement constraints. The optimal solution to the control problem may be achieved by nonlinear programming. However, this requires the full length of the time series of the surface elevation to be known. For irregular sea states this can only be predicted at most one peak period ahead of the time where any control strategy is applied. As a consequence, any realizable control strategy is necessary. The nonlinear programming solution is applied as a benchmark for the validation of the suggested control. The paper is organized as follows. In Section 2.1 the basic motion equation of point absorber is presented. In Section 2.2 the optimal control law for a point absorber with constraints on the displacement is derived and the obtained solution is benchmarked against a numerical solution from nonlinear programming. The obtained control law has feedback from further velocities and depends on the further wave load. The quantities need to be predicted at the time the control is applied, which is dealt with in Section 2.3. Finally, in Section 3 a numerical example is provided to investigate the quality of the theory.

2. Methodology

2.1. Equation of motion of point absorber

The heave absorber to be analyzed is shown in Fig. 1. An (x, y, z)-coordinate system is introduced with the origin O placed in the mean water level (MWL) at the centerline of the point absorber. The horizontal x-axis is oriented in the direction of the wave propagation, and the vertical z-axis is oriented in the upward direction. Only two-dimensional (plane) irregular waves are considered. The motion $v(t)$ of the body in the z-direction is measured from the static equilibrium state with no wave motion, where the static buoyancy force $f_{b,0}$ balances the gravity force mg and a possible static pre-stressing force from the mooring system $f_{p,0}$. g is the acceleration of gravity, and m indicates the structural mass including ballast.

In the dynamic state caused by the surface elevation $\eta(t)$ the indicated static forces disappear from the dynamic equation of motion. Assuming linear wave theory, $v(t)$ is given by the following linear integro-differential equation [10]:

$$M\ddot{v}(t) + r(v(t)) + \int_{t_0}^{t} h_{r\dot{v}}(t - \tau)\dot{v}(\tau)\,d\tau = f_e(t) - f_c(t) \ , \ t \in [t_0, t_1]$$
$$v(t_0) = v_0, \quad \dot{v}(t_0) = \dot{v}_0 \tag{1}$$

$f_e(t)$ is the wave excitation force on the absorber, and $f_c(t)$ is the reaction force from the power take-off system, which is used to control the motion of the absorber. The signs of $f_e(t)$ and $f_c(t)$ are defined in Fig. 1.

$r(v(t))$ is the quasi-static restoring force due to the buoyancy and the mooring system, caused by displacements from the static equilibrium state. Assuming small vertical vibrations, $r(v(t))$ may be linearized around the static equilibrium state as:

$$f_b(t) = -k\,v(t), \quad k = r'(0) \tag{2}$$

In the numerical results below the linearized relation in Eq. (7) has been assumed with the value of k given in Table 1.

$M = m + m_h$, where m_h indicates the added water mass at infinite high frequencies. v_0 and $\dot{v}_0$ are given initial conditions at the time t_0. t_1 is the terminal time of the control.

The impulse response function $h_{r\dot{v}}(t)$ in the convolution integral is causal, i.e. $h_{r\dot{v}}(t) = 0, \ t < 0$. The related frequency response function becomes [11]:

$$H_{r\dot{v}}(\omega) = \int_0^{\infty} \mathrm{e}^{-i\omega t}\, h_{r\dot{v}}(t)\, \mathrm{d}t \tag{3}$$

Fig. 2 shows the impulse response function $h_{r\dot{v}}(t)$ and the frequency response function $H_{r\dot{v}}(\omega)$ for the radiation force, based on the data of the absorber indicated in Table 1 in the numerical example below. In Fig. 2a the time has been normalized with respect to the peak period T_p. As seen, $h_{r\dot{v}}(t)$ effec-
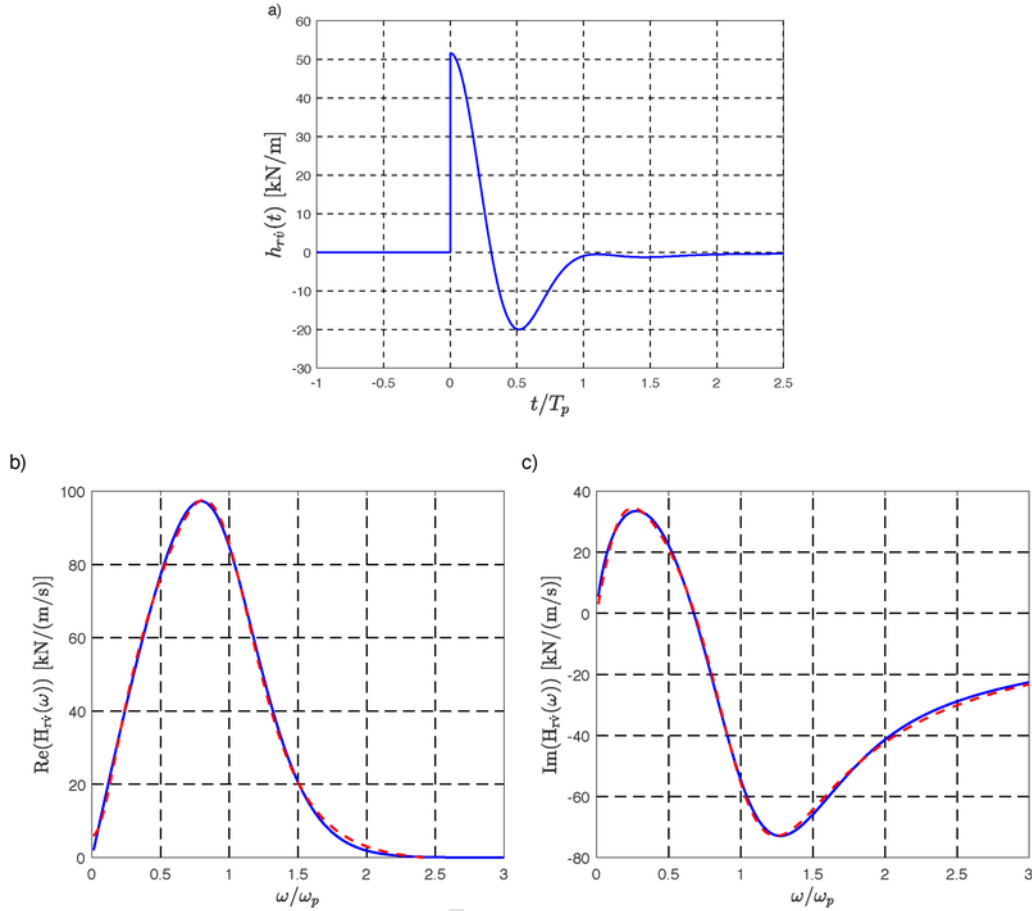
Fig. 2. Radiation force. (a) Impulse response function, $h_{r\dot{v}}(t)$. (b) Real part $\mathrm{Re}(H_{r\dot{v}}(\omega))$ of frequency response function. (c) Imaginary part $\mathrm{Im}(H_{r\dot{v}}(\omega))$ of frequency response function. ████████ : Numerical determined target. ████████ : Rational approximation of order $(m, n) = (2, 3)$.
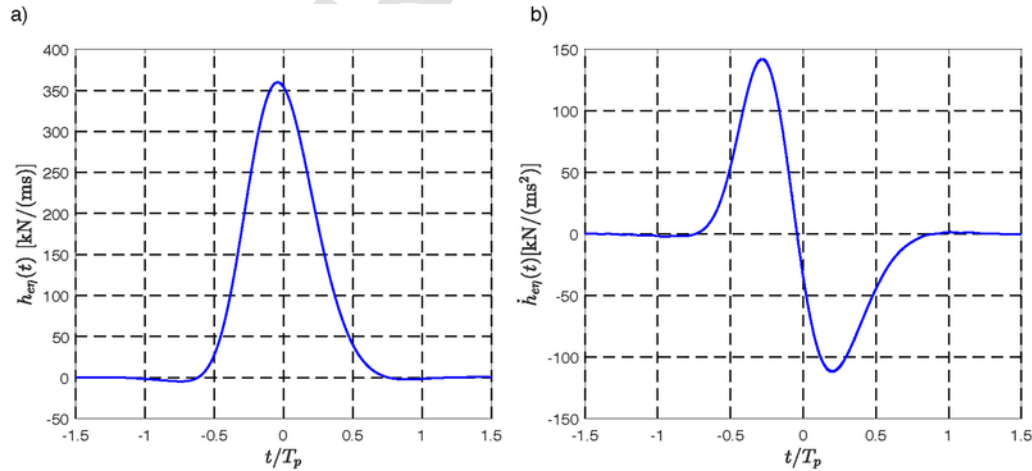

Fig. 3. Impulse response functions for wave excitation force. (a) $h_{e\eta}(t)$. (b) $\dot{h}_{e\eta}(t)$.

tively vanishes for $t > T_{\dot{v}}$, $T_{\dot{v}} \simeq T_p$. Below, it is shown that $T_{\dot{v}}$ indicates the prediction horizon of future velocities affecting the optimal control force in the unconstrained case. The angular frequency ω in Fig. 2b and c has been normalized with respect to the peak angular frequency $\omega_p = \frac{2\pi}{T_p}$. Since the real part is an even function of ω, and the imaginary part an odd function of ω, only re-

sults for positive values of the angular frequencies have been indicated. Further, the frequency response function $H_{r\dot{v}}(\omega)$ is approximated by a rational function of the order (m, n), where m and n indicate the order of the numerator and the denominator polynomials, respectively. The details of the approach can
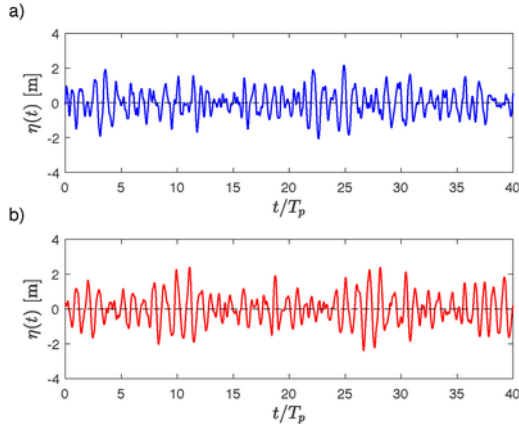
Fig. 4. Realizations of the surface elevation process $\eta(t)$, $H_s = 3.00$ m, $T_p = 7.42$ s. (a) $\gamma = 1$. (b) $\gamma = 5$.

be found in Appendix B. The rational approximation to $H_{r\dot{v}}(\omega)$ of order $(m, n) = (2, 3)$ has been illustrated in Fig. 2b and c.

The wave excitation force $f_e(t)$ may be expressed in terms of the following convolution integral of the sea-surface elevation $\eta(t)$ [12]:

$$f_e(t) = \int_{-\infty}^{\infty} h_{e\eta}(t - \tau)\, \eta(\tau)\, d\tau \tag{4}$$

The sea-surface elevation $\eta(t)$ is assumed to be observed at a sufficient distant position from the absorber, where the measurement is not disturbed by the radiation wave.

The time derivative of the wave excitation force, $\dot{f}_e(t)$, is given as:

$$\dot{f}_e(t) = \int_{-\infty}^{\infty} \dot{h}_{e\eta}(t - \tau)\, \eta(\tau)\, d\tau \tag{5}$$

Alternatively, $\dot{f}_e(t)$ may be obtained by numerical differentiation of the realizations of $f_e(t)$. $\dot{f}_e(t)$ is later used in the devised prediction algorithm for the wave excitation force.

The impulse response function $\dot{h}_{e\eta}(t)$ in Eq. (5) may be calculated from the following Fourier transform [11]:

$$\dot{h}_{e\eta}(t) = \frac{1}{2\pi} \int_{-\infty}^{\infty} e^{i\omega t}\, i\omega\, H_{e\eta}(\omega)\, d\omega \tag{6}$$

where $H_{e\eta}(\omega)$ indicates the frequency response function for the wave force, which can be calculated numerically by a boundary element method. In the present paper, the WAMIT program [13] has been applied.
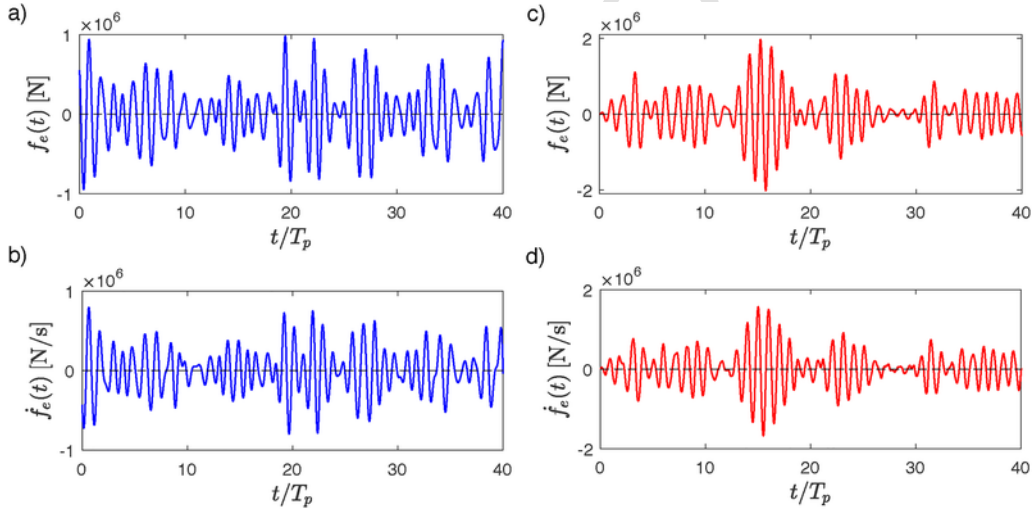

Fig. 5. Realizations of the wave excitation force process $f_e(t)$ and its derivative $\dot{f}_e(t)$, $H_s = 3.00$ m, $T_p = 7.42$ s. (a, b) $\gamma = 1$. (c, d) $\gamma = 5$.
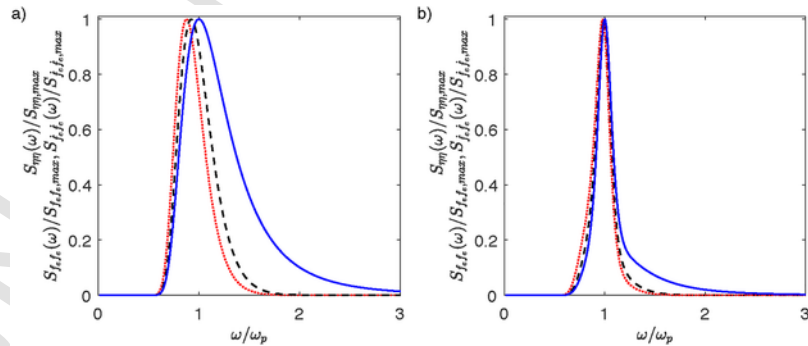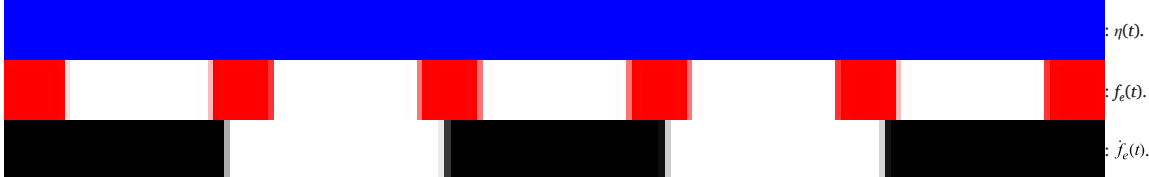

Fig. 6. Normalized double-sided auto-spectral density functions of $\eta(t), f_e(t), \dot{f}_e(t)$. (a) $\gamma = 1$. (b) $\gamma = 5$.

: $\eta(t)$.
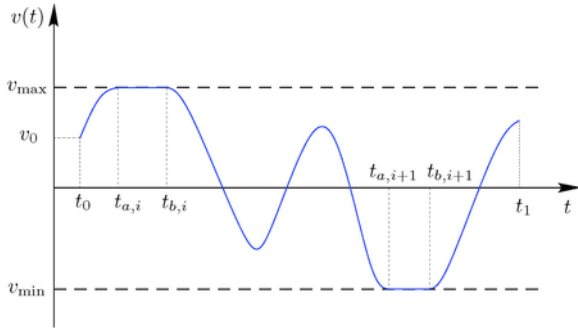
: $f_e(t)$.

: $\dot{f}_e(t)$.

Fig. 7. Constrained displacement response. Definition of parameters.

Fig. 3 shows the impulse response function $h_{e\eta}(t)$ and $\dot{h}_{e\eta}(t)$ for the considered point absorber. As seen, both impulse response functions effectively vanishes for $|t| > T_{f_e}$, $T_{f_e} \simeq 0.7\,T_p$. T_{f_e} indicates the prediction horizon for the wave excitation force.

Fig. 4a and b show simulated realizations of the Gaussian surface elevation process $\eta(t)$ defined by the double-sided JONSWAP auto-spectral density function given by Eq. (29) with the the indicated values of the significant wave height H_s and the peak period T_p, and with the bandwidth parameters $\gamma = 1$ and $\gamma = 5$, respectively. $\gamma = 1$ specifies the sea-state in open sea with unlimited fetch, whereas $\gamma = 5$ applies to a relatively small fetch.

Fig. 5a and c show realizations of the wave excitation force process $f_e(t)$ for $\gamma = 1$ and $\gamma = 5$, respectively, as calculated by Eq. (4) based on the corresponding realizations of the surface elevation process $\eta(t)$ shown in Fig. 4. Fig. 5b and d show the corresponding realization of the time derivative $\dot{f}_e(t)$. As seen, the realizations of $f_e(t)$ and $\dot{f}_e(t)$ are significantly more narrow-banded than the underlying surface elevations realizations. The double-sided auto-spectral density functions of the surface elevation $\eta(t)$, the wave load $f_e(t)$ and its time derivative $\dot{f}_e(t)$ have been shown in Fig. 6a and b for the wave spectrum bandwidth parameters $\gamma = 1$ and $\gamma = 5$ indicating broadbanded and narrowbanded sea-states, respectively. As seen, the wave spectrum $S_{\eta\eta}(\omega)$ is significantly more broadbanded than $S_{f_e f_e}(\omega)$ and $S_{\dot{f}_e \dot{f}_e}(\omega)$ for both cases of γ. This observation will be used in the estimation algorithm of the wave excitation force $f_e(t)$ presented in Section 2.3.1.
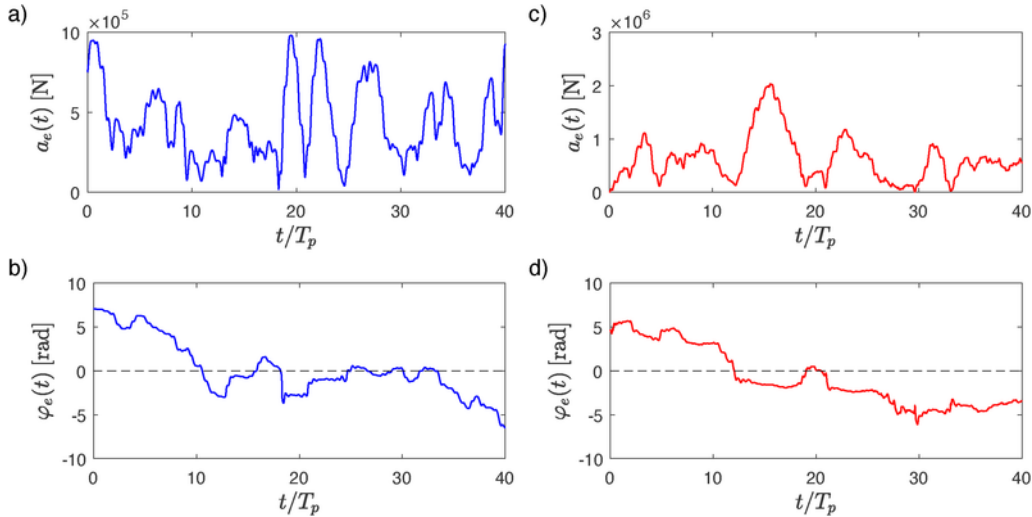

Fig. 8. Time-series of amplitude process $a_e(t)$ and phase process $\varphi_e(t)$, $H_s = 3.00$ m, $T_p = 7.42$ s. (a, b) $\gamma = 1$. (c, d) $\gamma = 5$.
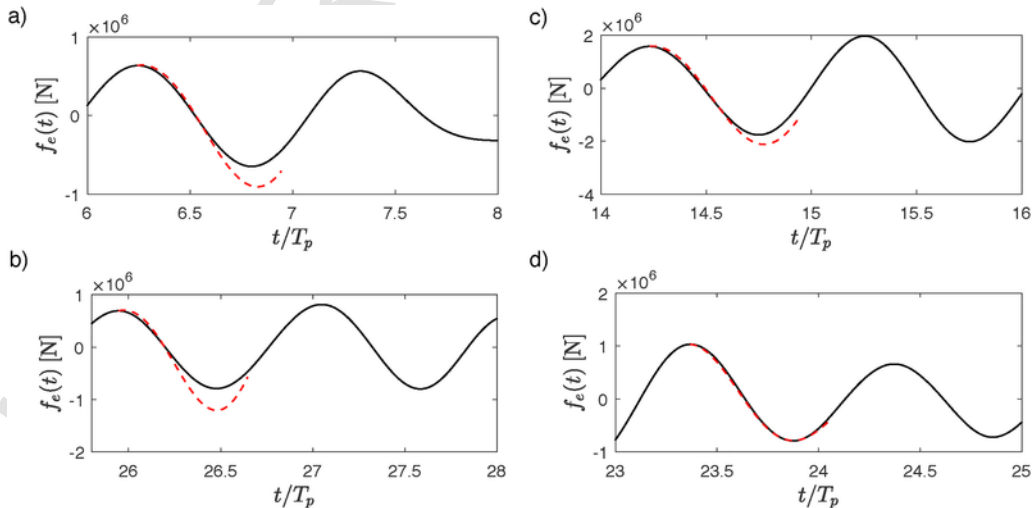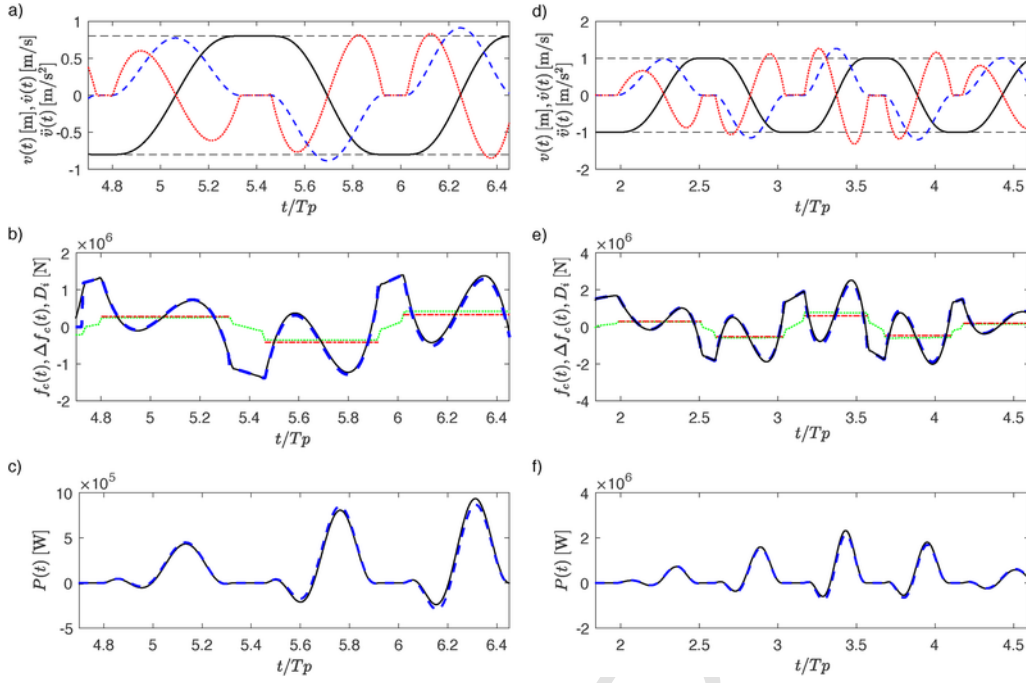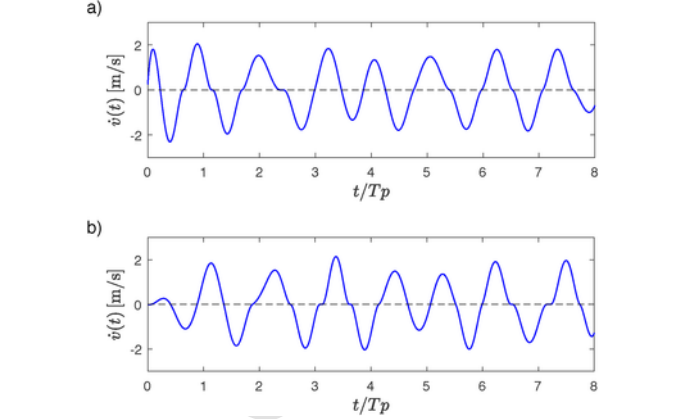

Fig. 9. Prediction of wave excitation force $f_e(t)$. (a, b) $\gamma = 1$. (c, d) $\gamma = 5$. _____: Nonlinear programming solution. _____: Predicted wave load.

Fig. 12. Time-series of $v(t)$, $\dot{v}(t)$, $\ddot{v}(t)$, control force $f_c(t)$ and instantaneous absorbed power $P(t)$ at optimal control, $H_s = 3.00$ m, $T_p = 7.42$ s. (a–c) $\gamma = 1$, $v_{\max} = -v_{\min} = 0.8$ m. (d–f) $\gamma = 5$, $v_{\max} = -v_{\min} = 1$ m. (a, d) ————: $v(t)$. ————: $\dot{v}(t)$. ————: $\ddot{v}(t)$. (b, e) ————: Nonlinear programming solution. ————: $f_c(t)$. ————: $\Delta f_c(t)$. ————: D_i. (c, f) ————: Nonlinear programming solution. ————: $P(t)$.
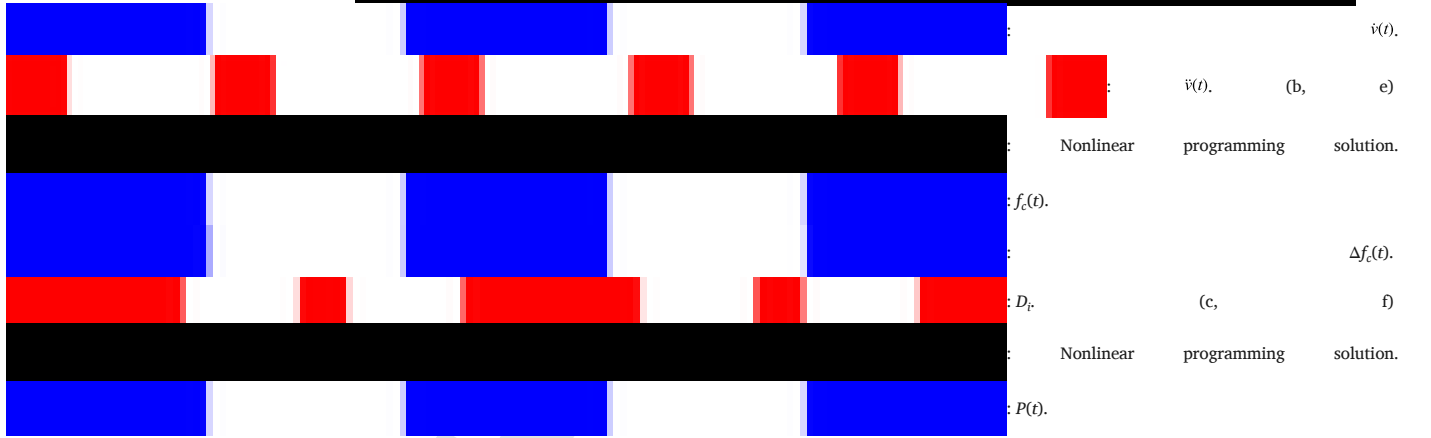
Fig. 10. Time-series of $\dot{v}(t)$, $H_s = 3.00$ m, $T_p = 7.42$ s, $v_{\max} = -v_{\min} = 2$ m. (a) $\gamma = 1$. (b) $\gamma = 5$.

2.2. Optimal control problem

The control problem for maximizing the absorbed power during the interval $]t_0, t_1]$ with constraints on the absorber displacement may be defined as:

$$
\left.
\begin{aligned}
\max J[\dot{v}, f_c] &= \int_{t_0}^{t_1} f_c(\tau)\dot{v}(\tau)\,d\tau \\
&\text{subject to the path constraint given by Eq. (1),} \\
&\text{and to the displacement constraint :} \\
&v_{\min} \leq v(t) \leq v_{\max}
\end{aligned}
\right\}
\tag{7}
$$

Let $v_{m,i}$ denote either $v_{\max}$ or $v_{\min}$, and let $[t_{a,i}, t_{b,i}]$ indicate the ith interval where the constrain $v_{m,i}$ is activated, see Fig. 7.

Since $\dot{v}(t) = \ddot{v}(t) = 0$ in the constraint intervals, the integro-differential equation (1) provides the following relation for the control force for $t \in [t_{a,i}, t_{b,i}]$:

$$
f_c(t) = f_e(t) + C_i
\tag{8}
$$

where C_i is a constant given as:
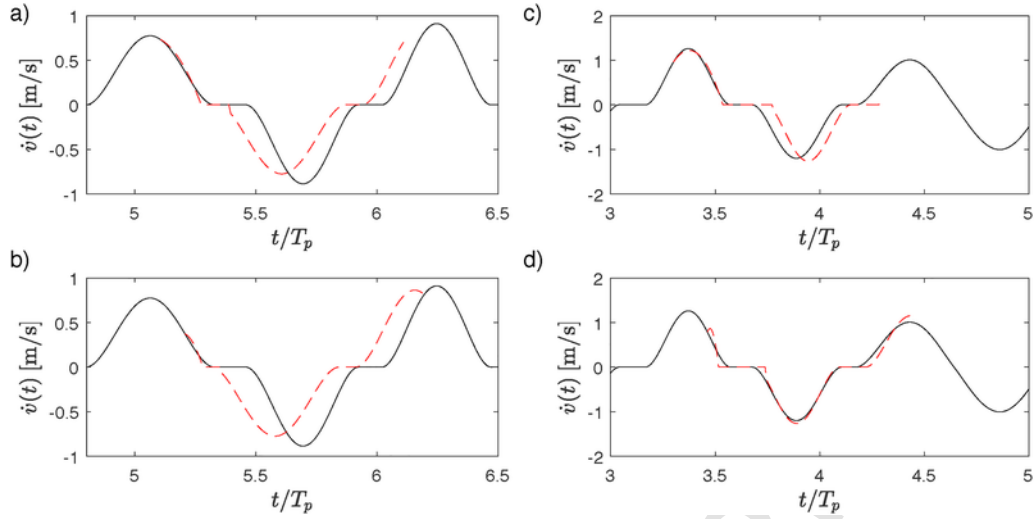
Fig. 11. Prediction of $\dot{v}(t)$, $H_s = 3.00$ m, $T_p = 7.42$ s. (a, b) $\gamma = 1$, $v_{max} = -v_{min} = 0.8$ m. (c, d) $\gamma = 5$, $v_{max} = -v_{min} = 1$ m. ——: Nonlinear programming solution. - - - -: Predicted velocity.
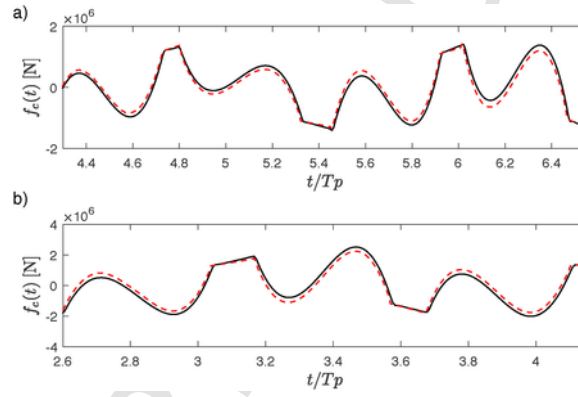
Fig. 13. Prediction of $f_c(t)$, $H_s = 3.00$ m, $T_p = 7.42$ s. (a) $\gamma = 1$, $v_{max} = -v_{min} = 0.8$ m. (b) $\gamma = 5$, $v_{max} = -v_{min} = 1$ m. ——: Nonlinear programming. - - - -: Predicted control force.
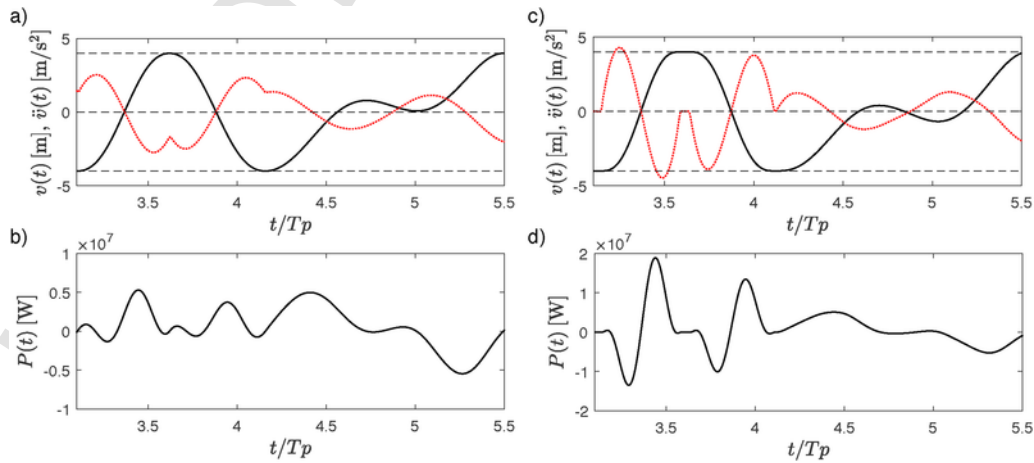
Fig. 14. Time-series of $v(t)$, $\ddot{v}(t)$ and instantaneous absorbed power $P(t)$ at optimal control, $\gamma = 5$, $H_s = 3.00$ m, $T_p = 7.42$ s, $v_{max} = -v_{min} = 4$ m. (a, b) $\Delta\tau = 0.05$s. (c, d) $\Delta\tau = 0.01$s.
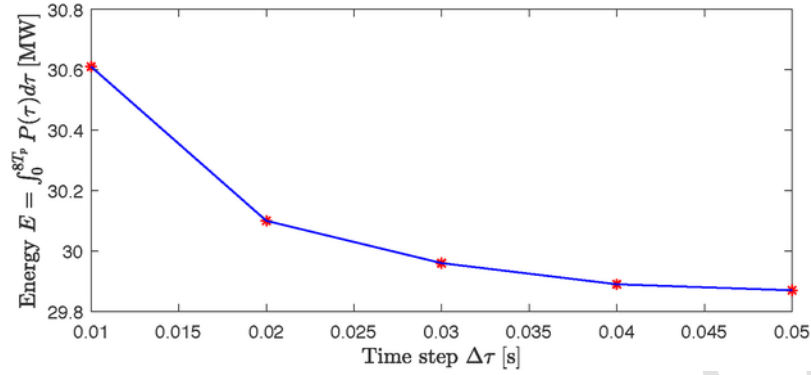
Fig. 15. Variation of the absorbed energy with different time step $\Delta\tau$.

$$C_i = -\int_{t_0}^{t_{a,i}} h_{r\dot{v}}(t_{a,i} - \tau)\,\dot{v}(\tau)\,d\tau - r(v_{m,i}) \tag{9}$$

Assume that $\dot{v}(t)$ is observed continuously in the interval $[t_0, t_{a,i}[$. Then, C_i can be calculated by Eq. (9).

Eq. (8) indicates that the optimal control law is of the open loop type, whenever the displacement constraint is active. Hence, the wave excitation force $f_e(t)$ needs to be estimated in these intervals.

The corresponding optimal control problem in the interval $]t_{b,i}$, $t_{a,i+1}[$, where no constraint is active, has previously been solved by the authors [14]. The solution may be given as:

$$f_c(t) = f_{c,0}(t) + D_i \tag{10}$$

where:

$$f_{c,0}(t) = -M\dot{v}(t) + \int_t^{t_1} h_{r\dot{v}}(\tau - t)\,\dot{v}(\tau)\,d\tau - r(v(t)) \tag{11}$$

D_i is a constant, which can be calibrated at the interface to the previous constrained interval. From Eqs. (8) and (10) follows:

$$f_c(t_{b,i}) = f_e(t_{b,i}) + C_i = f_{c,0}(t_{b,i}) + D_i \tag{12}$$

Similarly, we have for the previous unconstrained interval at the boundary at $t = t_{a,i}$:

$$f_c(t_{a,i}) = f_e(t_{a,i}) + C_i = f_{c,0}(t_{a,i}) + D_{i-1} \tag{13}$$

Since, $f_{c,0}(t_{a,i}) = f_{c,0}(t_{b,i})$ it follows from Eqs. (12) and (13):

$$D_i = D_{i-1} + f_e(t_{a,i}) - f_e(t_{b,i}), \quad i = 1, 2, \ldots \tag{14}$$

$f_c(t) = f_{c,0}(t)$ during the first unconstrained interval $[t_0, t_{a,1}]$, so $D_0 = 0$. Hence, Eq. (14) provides a recursive relation for the determination of the constants D_i, if the wave excitation force at the boundaries of the constrained intervals can be determined.

Due to accumulated estimation errors of the wave excitation forces, Eq. (14) becomes increasingly inaccurate. To remedy this, D_i should occasionally be calculated directly from Eq. (12) leading to:

$$D_i = f_e(t_{b,i}) + C_i - \int_{t_{b,i}}^{t_1} h_{r\dot{v}}(\tau - t_{b,i})\,\dot{v}(\tau)\,d\tau + r(v_{m,i}) \tag{15}$$

where it has been used that $\dot{v}(t_{b,i}) = 0$ in the expression for $f_{c,0}(t_{b,i})$ given by Eq. (11). Eq. (15) requires a prediction of $\dot{v}(\tau), \tau \in [t_{b,i}, t_{b,i} + T_{\dot{v}}]$.

2.3. Estimation and prediction problems

The solution for the optimal control law $f_c(t)$ as given by Eqs. (8)–(12) requires that the wave excitation force $f_e(t)$ can be estimated during the constrained time intervals, cf. Eq. (8). In the unconstrained intervals the evaluation

of the function $f_{c,0}(t)$ given by Eq. (11) requires that the velocity $\dot{v}(\tau)$ ahead of the present time t to be predicted. Because the support of the impulse response function $h_{r\dot{v}}$ is effectively confined to the interval $[0, T_p]$, the prediction horizon is limited to $T_{\dot{v}} \simeq T_p$, cf. Fig. 2a.

The estimation and prediction procedures described below presume that the surface elevation $\eta(t)$ and the vertical acceleration $\ddot{v}(t)$ of the absorber are continuously measured. The displacement $v(t)$ and velocity $\dot{v}(t)$ are obtained by online integration of the acceleration signal.

2.3.1. Estimation of wave excitation force

The wave excitation force and its derivative at the time $t - T_{f_e}$ may be written as, cf. Eqs. (4) and (6):

$$\left.\begin{aligned} f_e(t - T_{f_e}) &\simeq \int_{-\infty}^t h_{e\eta}(t - T_{f_e} - \tau)\,\eta(\tau)\,d\tau \\ \dot{f}_e(t - T_{f_e}) &\simeq \int_{-\infty}^t \dot{h}_{e\eta}(t - T_{f_e} - \tau)\,\eta(\tau)\,d\tau \end{aligned}\right\} \tag{16}$$

Eq. (16) is based on the fact that $h_{e\eta}(-T_{f_e}) \simeq \dot{h}_{e\eta}(-T_{f_e}) \simeq 0$, cf. Fig. 3a and b, so surface elevations beyond the time t will not affect the left-hand sides of Eq. (16). Further, the surface elevation $\eta(\tau)$ is available up to and including the time t.

$f_e(t)$ and $\dot{f}_e(t)$ may be represented by a van der Pol transformation defined as, [15]:

$$\left.\begin{aligned} f_e(t) &= a_e(t)\,\cos(\omega_p t + \varphi_e(t)) \\ \dot{f}_e(t) &= -\omega_p\,a_e(t)\,\sin(\omega_p t + \varphi_e(t)) \end{aligned}\right\} \tag{17}$$

where the amplitude process $a_e(t)$ and the phase process $\varphi_e(t)$ are given as:

$$\left.\begin{aligned} a_e(t) &= \sqrt{f_e^2(t) + \left(\frac{\dot{f}_e(t)}{\omega_p}\right)^2} \\ \varphi_e(t) &= \arctan\left(-\frac{\dot{f}_e(t)}{\omega_p f_e(t)}\right) - \omega_p t \end{aligned}\right\} \tag{18}$$

Because $f_e(t)$ and $\dot{f}_e(t)$ are narrow-banded stochastic processes, $a_e(t)$ and the $\varphi_e(t)$ become slowly varying functions with time. Alternatively, the Hilbert-Huang transform may be used, where $\frac{\dot{f}_e(t)}{\omega_p}$ is replaced by the Hilbert transform $\hat{f}_e(t)$ [16,17]. Actually, these alternatives are equivalent for harmonic varying signals.

Fig. 8 shows the realizations of $a_e(t)$ and $\varphi_e(t)$ for $\gamma = 1$ and $\gamma = 5$, respectively, based on the realizations of $f_e(t)$ and $\dot{f}_e(t)$ shown in Fig. 5.

Define the following quantities:

$$\left.\begin{aligned} a_{-j} &= a_e(t - T_{f_e} - j\,T_p) \\ \varphi_{-j} &= \varphi_e(t - T_{f_e} - j\,T_p) \end{aligned}\right\}, \quad j = 0, 1, 2, \ldots \tag{19}$$

Next, the values of $a_e(\tau)$ and $\varphi_e(\tau)$ for $\tau \in]t - T_{fe}, t]$ are estimated by extrapolation from $\tau = t - T$ by means of 2nd order Lagrange polynomials calibrated by the function values at $t - T_{fe}$, $t - T_{fe} - T_p$ and $t - T_{fe} - 2T_p$, given as:

$$
\begin{aligned}
a_e(\tau) &= a_0 &&+ \tfrac{1}{2}\left(3a_0 - 4a_{-1} + a_{-2}\right)u &&+ \tfrac{1}{2}\left(a_0 - 2a_{-1} + a_{-2}\right)u^2 \\
\varphi_e(\tau) &= \varphi_0 &&+ \tfrac{1}{2}\left(3\varphi_0 - 4\varphi_{-1} + \varphi_{-2}\right)u &&+ \tfrac{1}{2}\left(\varphi_0 - 2\varphi_{-1} + \varphi_{-2}\right)u^2
\end{aligned}
$$

where

$$
u = \frac{\tau - t + T_{fe}}{T_p} \tag{21}
$$

Then, $f_e(\tau)$ in the interval $]t - T_{fe}, t]$ is predicted from:

$$
f_e(\tau) = a_e(\tau)\cos(\omega_p \tau + \varphi_e(\tau)) \tag{22}
$$

Fig. 9 illustrates prediction results for the wave excitation force $f_e(t)$ one prediction period $T_{fe} = 0.7T_p$ ahead. Fig. 9a and b show predictions for $\gamma = 1$ at the instants of time $t = 6.2T_p$ and $t = 25.9T_p$ on the time-series shown in Fig. 5a. Fig. 9c and d show similar results for $\gamma = 5$ predicted at the instants of time $t = 14.2T_p$ and $t = 23.4T_p$ on the time-series shown in Fig. 5c. The predictions are more accurate for $\gamma = 5$, due to the enhanced narrow-bandedness of the time-series in this case.

2.3.2. Prediction of future velocities

The velocity response in the vicinity to the constrained interval is significantly influenced by the initial values $\dot{v}(t_{b,i}) = 0$. This initial values needs to be taken into consideration at the prediction of $\dot{v}(t)$, $t > t_{b,i}$.

As seen from Fig. 12a and b, $\dot{v}(t)$ is approximately skew-symmetric before and after the constrained interval $[t_{a,i}, t_{b,i}]$ corresponding to the relation:

$$
\dot{v}(t) \simeq -\dot{v}(t_{a,i} + t_{b,i} - t), \quad t \in [t_{b,i}, t_{b,i} + T_{\dot{v}}] \tag{23}
$$

The right hand side of Eq. (23) is available from previous measurements of the velocity response. Hence, Eq. (23) may be used to evaluate $f_{c,0}(t)$ for $t \in]t_{b,i}, t_{b,i} + T_{\dot{v}}]$. Further, the constant D_i given by Eq. (15) may be approximated as:

$$
\begin{aligned}
D_i &\simeq f_e(t_{b_i}) + C_i - \int_{t_{b_i}}^{t_{b,i}+T_{\dot{v}}} h_{r\dot{v}}(\tau - t_{b_i})\,\dot{v}(\tau)\,d\tau + r(v_{m,i}) \\
&\simeq f_e(t_{b_i}) + C_i + \int_{t_{a_i}-T_{\dot{v}}}^{t_{a_i}} h_{r\dot{v}}(t_{a_i} - \tau)\,\dot{v}(\tau)\,d\tau + r(v_{m,i})
\end{aligned} \tag{24}
$$

Around one prediction interval $T_{\dot{v}}$ away from the constraints, corresponding to the time interval $[t_{b,i} + T_{\dot{v}}, t_{a,i+1} - T_{\dot{v}}]$, the response processes $v(t)$ and $\dot{v}(t)$ become stationary and narrow-banded for both $\gamma = 1$ and $\gamma = 5$, see Fig. 10. $v(t)$ is at an absolute extremum, when the displacement constraints are active, and may have one or more local maxima or minima between these states. At any of these extremes the velocity $\dot{v}(t) = 0$. As seen from Fig. 10, $\dot{v}(t)$ have exactly one local maximum or local minimum between the zeros, which is characterizing a narrow-banded response [11].

Then, velocities $\dot{v}(\tau)$, $\tau \in]t, t + T_{\dot{v}}]$ ahead of the present time t may be predicted by based on a van der Pol transformation similar to the one used for predictions of future wave excitation forces defined by Eqs. (17) and (18):

$$
\left.\begin{aligned}
v(t) &= a_v(t)\cos(\omega_p t + \varphi_v(t)) \\
\dot{v}(t) &= -\omega_p a_v(t)\sin(\omega_p t + \varphi_v(t))
\end{aligned}\right\} \tag{25}
$$

where the slowly varying amplitude process $a_v(t)$ and the phase process $\varphi_v(t)$ given as:

$$
\left.\begin{aligned}
a_v(t) &= \sqrt{v^2(t) + \left(\frac{\dot{v}(t)}{\omega_p}\right)^2} \\
\varphi_v(t) &= \arctan\left(-\frac{\dot{v}(t)}{\omega_p v(t)}\right) - \omega_p t
\end{aligned}\right\} \tag{26}
$$

At a certain instant of time t is checked whether the predicted displacement exceeds the boundaries during the prediction interval $[t, t + T_p]$. If so, the time $t_{a,i+1}$ is estimated from the prediction, and a cubic interpolation is applied for $v(t)$ in the interval $[t, t_{a,i+1}]$, given as:

$$
\begin{aligned}
v(\tau) &= v(t) + \dot{v}(t)(\tau - t_{a,i+1}) \\
&\quad + a(\tau - t_{a,i+1})^2 + b(\tau - t_{a,i+1})^3
\end{aligned} \tag{27}
$$

where

$$
\left.\begin{aligned}
a &= \frac{1}{(t_{a,i+1}-t_0)^2}\left(3\left(v_{m,i+1} - v(t)\right) + 2\dot{v}(t)\left(t_{a,i+1} - t\right)\right) \\
b &= \frac{1}{(t_{a,i+1}-t_0)^3}\left(-2\left(v_{m,i+1} - v(t)\right) + \dot{v}(t)\left(t_{a,i+1} - t\right)\right)
\end{aligned}\right\} \tag{28}
$$

a and b are determined so $v(t_{a,i+1}) = v_{m,i+1}$ and $\dot{v}(t_{a,i+1}) = 0$.

Finally, the predicted velocity in the interval $[t_{a,i+1} - T_{\dot{v}}, t_{a,i+1}]$ can be obtained by the derivative of the displacement indicated in Eq. (27). Combination with the skew-symmetric property of the velocity indicated in Eq. (23), the predicted velocity at least one period ahead can be obtained. Fig. 11 shows the predicted velocities for $\gamma = 1$ and $\gamma = 5$, separately.

3. Numerical example

A point heave wave energy converter indicated in Fig. 1 is considered in the numerical simulation. The relevant data of the absorber and the wave excitation parameters have been indicated in Table 1.

$S_{\eta\eta}(\omega)$ is taken as the double-sided JONSWAP auto spectral density function given as [18]:

$$
S_{\eta\eta}(\omega) = \delta\,\frac{H_s^2}{\omega_p}\,\gamma^{\beta}\left(\frac{|\omega|}{\omega_p}\right)^{-5}\exp\left(-\frac{5}{4}\left(\frac{\omega}{\omega_p}\right)^{-4}\right) \tag{29}
$$

where

$$
\left.\begin{aligned}
\delta &= \frac{0.0312}{0.230 + 0.0336\,\gamma - \frac{0.185}{1.9+\gamma}} \\
\beta &= \exp\left(-\frac{1}{2}\left(\frac{|\omega|-\omega_p}{\sigma\,\omega_p}\right)^2\right) \\
\sigma &= \begin{cases} 0.07, & |\omega| \le \omega_p \\ 0.09, & |\omega| > \omega_p \end{cases}
\end{aligned}\right\} \tag{30}
$$

T_p is the peak period, $\omega_p = \frac{2\pi}{T_p}$ is the related angular peak frequency and H_s is the significant wave height. γ is the so-called peak enhancement parameter which controls the bandwidth of the spectrum.

The validity of the theoretical optimal control solution given by Eqs. (8)–(12) has been verified by comparison to a numerical solution obtained by the nonlinear programming algorithm described in Appendix A.

Fig. 12a and d show the trajectories of $v(t)$, $\dot{v}(t)$, $\ddot{v}(t)$ with the displacement constraints $v_{\max} = -v_{\min} = 0.8\,\text{m}$ and $v_{\max} = -v_{\min} = 1.0\,\text{m}$ at optimal control determined by the nonlinear programming algorithm for $\gamma = 1$ and $\gamma = 5$, respectively. The nonlinear programming solutions are merely available at discrete points separated at the distance $\Delta t = \frac{T_p}{150}$.

Because, the first and second derivative of the displacement response and the first derivative of the velocity response vanish in the constrain intervals $[t_{a,i}, t_{b,i}]$, these responses are flat at the boundaries of these intervals. Hence, neither of these responses are suitable for identifying the times $t_{a,i}$ and $t_{b,i}$, which are essential to the devised control algorithm. Instead, $t_{a,i}$ and $t_{b,i}$ should be determined from the observed time series of the acceleration response which has an early detected discontinuous change of slope at the entrance and exit of the constrained interval as shown in Fig. 7a and d. Further, the velocity response between the constrained intervals turns out to be significantly narrow-banded. This observation will be used in the estimation algorithm of the unconstrained control force $f_{c,0}(t)$ given by Eq. (11).

Fig. 12b and e show the variation with time of the optimal control force $f_c(t)$ and the theoretical solution given by Eqs. (8)–(12) for $\gamma = 1$ and $\gamma = 5$, respectively, using the optimal response trajectories shown in Fig. 7a and d in the theoretical solution. Also shown in the figure is the difference $\Delta f_c(t) = f_c(t) - f_{c,0}(t)$ between the constrained intervals. According to Eq. (11) this difference is given by the constant D_i. The small deviation between these is assumed to be caused by uncertainty in the determination of the boundaries t_{a_i} and $t_{b,i}$ of the constrained interval from the available discrete time specification of $\ddot{v}(t)$. As seen, the estimate of D_i is valid up to and including the time $t_{a,i+1}$, although this constant has been calibrated at the time $t_{b,i}$ at the end of the previous constrained interval.

Fig. 12c and f show the variation with time of the instantaneous absorbed power $P(t) = f_c(t)\dot{v}(t)$ at optimal control for $\gamma = 1$ and $\gamma = 5$, respectively. The deviation is quite insignificant.

Summing up, the devised control algorithm for optimal power take-off requires the sequence of constants C_i and D_i to be determined, along with estimation of the wave load $f_e(t)$ and the unconstrained control force $f_{c,0}(t)$. C_i is obtained from Eq. (9) and D_i from Eq. (14) or Eq. (15). The instants of time for entrance and exit of the constrained intervals is most reliable obtained from observation of the acceleration signal.

Based on Eqs. (10) and (24) the control force for unconstrained parts can be obtained. The constrained parts can be determined from the continuous measurement of the responses of the absorber. Fig. 13 shows the predicted control forces for $\gamma = 1$ and $\gamma = 5$. As seen, a good agreement is shown in Fig. 13.

Here the influence of the deviation of the predicted control force on the trajectory will not be considered. It assumed that the acceleration of the absorber can be measured continuously. Correspondingly, the times $t_{a,i}$ and $t_{b,i}$ can be determined in real time.

4. Conclusions

The paper presents a semi-analytical solution for the optimal power take-off of a heave point wave energy converter with the constrained displacements. The solution requires that the wave excitation force can be estimated during active displacement constraints, and that the velocity response between constrained states can be predicted at least one wave period ahead. To handle these problems physical based estimation and prediction algorithms have been devised, which make use of the narrow-banded character of the wave excitation force and the unconstrained velocity response. The obtained control law has been verified against numerical solutions based on nonlinear programming for relatively broad-banded and narrow-banded sea states. In both cases a good agreement is obtained.

Acknowledgements

Appendix A. Nonlinear programming algorithm

The optimal control problem in Eq. (7) is reformulated as a nonlinear programming problem by discretizing the objective functional and the state vector in time:

$$\max \quad J(\mathbf{X}(\tau_M)) = x_{n+3}(\tau_M)$$

subject to the path and inequality constraints :

$$\mathbf{h}(\mathbf{X}(\tau_j)) = \left.\begin{array}{c} \mathbf{c}(\mathbf{X}(\tau_j)) = 0 \\ \begin{bmatrix} v(\tau_j) & -v_{\max} \\ -v(\tau_j) & +v_{\min} \end{bmatrix} - \mathbf{s}(\tau_j) = 0 \\ \mathbf{s}(\tau_j) \geq 0 \end{array}\right\} \tag{31}$$

where $\tau_j = t_0 + j\,\Delta\tau\; j = 0, 1, …, M$.

$\mathbf{s}(t)$ indicates a vector function of slack variables. The time step in the discretization of the interval $]t_0, t_1]$ is given as $\Delta\tau = \frac{t_1 - t_0}{M}$. The vector $\mathbf{X}(t)$ of dimension $2n + 6$ and the path constrain vector $\mathbf{c}(\mathbf{X}(t))$ of dimension $n + 3$ are de-

fined as:

$$\mathbf{X}(t) = \left[v(t), \dot{v}(t), \mathbf{z}_r^T(t), x_{n+3}(t), \frac{d}{dt}v(t), \frac{d}{dt}\dot{v}(t), \frac{d}{dt}\mathbf{z}_r^T(t), \frac{d}{dt}x_{n+3}(t)\right]^T \tag{32}$$

$$\mathbf{c}(\mathbf{X}(t))$$
$$= \begin{bmatrix} \frac{d}{dt}v(t) - \dot{v}(t) \\ M\frac{d}{dt}\dot{v}(t) + \mathbf{p}_r\,\mathbf{z}_r(t) + r(v(t)) - f_e(t) + f_c(t) \\ \frac{d}{dt}\mathbf{z}_r(t) - \mathbf{A}_r\,\mathbf{z}_r(t) - \mathbf{b}_r\,\dot{v}(t) \\ \frac{d}{dt}x_{n+3}(t) - f_c(t)\,\dot{v}(t) \end{bmatrix} \tag{33}$$

$\mathbf{z}_r(t)$ is a state vector, $\mathbf{A}_r$ is a quadratic matrix, and $\mathbf{b}_r$ and $\mathbf{p}_r$ are column and row vectors related to the convolution integral in Eq. (1), all defined in Appendix B.

The inherent approximation in the indicated nonlinear programming formulation concerns the discretization of the time continuous problem into $M + 1$ discrete instants of time for optimization, and the use of the rational approximation in Eq. (38) for the force $f_{r,0}(t)$.

The formulation applies to both displacement constraints and control force constraints. In case, merely control force constraints are prescribed the algorithm is applied by using large values of $v_{\max}$ and small values of $v_{\min}$.

The applied algorithm for solving the indicated nonlinear programming problem is described in El-Bakry et al. [19].

It should be noted that the optimal solution obtained by the nonlinear programming depends qualitatively and quantitatively on the applied time step $\Delta\tau$. Fig. 14a and c show the obtained time series of displacement $v(t)$ and the acceleration $\ddot{v}(t)$ for $v_{\max} = -v_{\min} = 4$m with the constraints checked the intervals $\Delta\tau = 0.05$s and $\Delta\tau = 0.01$s, respectively. In Fig. 14a, the acceleration is not zero when the displacement reaches the boundary, which means that the displacement constraint is not active in a finite time interval, and $v(t)$ is merely tangential to the constraint. In contrast, in Fig. 14c the constraint is everywhere active in a finite time interval, as assumed in the theory.

Fig. 14b and d indicate the instantaneous absorbed power $P(t)$ as predicted by the nonlinear programming algorithm during a control interval $[0, 8T_p]$ for the two time steps. The absorbed energy $E = \int P(\tau)d\tau$ during the interval becomes $E = 29.87$MJ for $\Delta\tau = 0.05$s and $E = 30.61$MJ for $\Delta\tau = 0.01$s. Actually, E turns out to be monotonously decreasing function of $\Delta\tau$, as shown in Fig. 15. The theoretical solution given by Eqs. (8) and (10) checks the constraints throughout the control interval $[t_0, t_1]$. Hence, it is expected that the nonlinear programming solutions approach the theoretical solution in the limit $\Delta\tau \to 0$.

Appendix B. State vector formulation of equation of motion

The nonlinear programming algorithm presumes a state vector description of the integro-differential equation of motion (1). To achieve this the frequency response function $\tilde{H}_{r\dot{v}}(\omega)$ given by Eq. (3) is approximated by a rational function:

$$\tilde{H}_{r\dot{v}}(\omega) = \frac{P(s)}{Q(s)}, \quad s = i\omega \tag{34}$$

$$\left.\begin{array}{ll} P(s) & = p_0 s^m + \cdots + p_{m-1}\,s + p_m \\ Q(s) & = s^n + q_1 s^{n-1} + \cdots + q_{n-1}\,s + q_n \\ & = (s - s_1)\cdots(s - s_{n-1})(s - s_n) \end{array}\right\} \tag{35}$$

where $m < n$. $p_0, …, p_m$ and $q_1, …, q_n$ are real constants determined, so $\tilde{H}_{r\dot{v}}(\omega)$ approximates the target frequency function $H_{r\dot{v}}(\omega)$ at best in some normed sense, and so the poles (roots of the denominator polynomial) $s_j, j = 1, …, n$ all have negative real part, $\mathrm{Re}(s_j) < 0$. The latter condition is the necessary and sufficient condition for causality and asymptotic stability of the filter defined by Eq. (34). A rational approximation of the order $(m, n) = (2, 3)$ has been shown with a dashed signature in Fig. 2b and c, and was used in the nonlinear programming analysis.

Consider the convolution integral:

$$f_{c,0}(t) = \int_{t_0}^{t} h_{r\dot{v}}(t-\tau)\,\dot{v}(\tau)\,d\tau \tag{36}$$

Then, $f_{r,0}(t)$ may be obtained as output to the following system of linear, ordinary filter differential equations driven by the velocity $\dot{v}(t)$:

$$\left.\begin{array}{l} f_{r,0}(t) = p_0\dfrac{d^m x(t)}{dt^m} + p_1\dfrac{d^{m-1}x(t)}{dt^{m-1}} + \cdots + p_{m-1}\dfrac{dx(t)}{dt} + p_m\,x(t) \\[2mm] \dfrac{d^n x(t)}{dt^n} + q_1\dfrac{d^{n-1}x(t)}{dt^{n-1}} + \cdots + q_{n-1}\dfrac{dx(t)}{dt} + q_n\,x(t) = \dot{v}(t) \end{array}\right\} \tag{37}$$

where $x(t)$ is an auxiliary response process without any physical interpretation.

Eq. (37) may be represented on the state vector form:

$$\left.\begin{array}{l} f_{r,0}(t) = \mathbf{p}_r\,\mathbf{z}_r(t) \\[1mm] \dfrac{d}{dt}\mathbf{z}_r(t) = \mathbf{A}_r\,\mathbf{z}_r(t) + \mathbf{b}_r\,\dot{v}(t), \quad t\in\,]t_0,t_1] \\[1mm] \mathbf{z}_r(t_0) = \mathbf{0} \end{array}\right\} \tag{38}$$

The initial value $\mathbf{z}_r(t_0) = \mathbf{0}$ follows because $f_{r,0}(t_0) = 0$.

The state vector $\mathbf{z}_r(t)$, the column vector $\mathbf{b}_r$, the system matrix $\mathbf{A}_r$ and the row vector $\mathbf{p}_r$ are given as:

$$\mathbf{z}_r(t) = \begin{bmatrix} x(t) \\ \frac{d}{dt}x(t) \\ \vdots \\ \frac{d^{n-2}}{dt^{n-2}}x(t) \\ \frac{d^{n-1}}{dt^{n-1}}x(t) \end{bmatrix}, \quad \mathbf{b}_r = \begin{bmatrix} 0 \\ 0 \\ \vdots \\ 0 \\ 1 \end{bmatrix}$$

$$\mathbf{A}_r = \begin{bmatrix} 0 & 1 & \cdots & 0 & 0 \\ 0 & 0 & \cdots & 0 & 0 \\ \vdots & \vdots & \ddots & \vdots & \vdots \\ 0 & 0 & \cdots & 0 & 1 \\ -q_n & -q_{n-1} & \cdots & -q_2 & -q_1 \end{bmatrix}$$

$$\mathbf{p}_r = [\,p_m \quad p_{m-1} \cdots p_1 \quad p_0 \quad 0 \cdots 0\,] \tag{39}$$

Then, Eq. (1) may be represented by the state vector differential equation:

$$\left.\begin{array}{l} \dfrac{d}{dt}\mathbf{z}(t) = \mathbf{g}(\mathbf{z}(t),f_c(t),t), \quad t\in[t_0,t_1] \\[1mm] \mathbf{z}(t_0) = \mathbf{z}_0 \end{array}\right\} \tag{40}$$

The state vector $\mathbf{z}(t)$, the initial value vector $\mathbf{z}_0$ and the right hand side of the state vector equation $\mathbf{g}(\mathbf{z}(t),f_c(t),t)$ are given as:

$$\mathbf{z}(t) = \begin{bmatrix} v(t) \\ \dot{v}(t) \\ \mathbf{z}_r(t) \end{bmatrix}, \quad \mathbf{z}_0 = \begin{bmatrix} v(t_0) \\ \dot{v}(t_0) \\ 0 \end{bmatrix} \tag{41}$$

$$\mathbf{g}(\mathbf{z}(t),f_c(t),t)$$
$$= \begin{bmatrix} \dot{v}(t) \\ \frac{1}{M}\left(-\mathbf{p}_r\mathbf{z}_r(t) - r(v(t)) + f_e(t) - f_c(t)\right) \\ \mathbf{A}_r\mathbf{z}_r(t) + \mathbf{b}_r\dot{v}(t) \end{bmatrix} \tag{42}$$

References

[1] R.F. Hartl, S.P. Sethi, R.G. Vickson, A survey of the maximum principles for optimal control problems with state constraints, SIAM Rev. 37 (2) (1995) 181–218.

[2] D.S. Naidu, Optimal Control Systems, CRC Press, 2002.

[3] D. Jacobson, M. Lee, A transformation technique for optimal control problems with a state variable inequality constraint, IEEE Trans. Autom. Control 14 (5) (1969) 457–464.

[4] L. Lasdon, S. Mitter, A. Waren, The conjugate gradient method for optimal control problems, IEEE Trans. Autom. Control 12 (2) (1967) 132–138.

[5] H. Eidsmoen, Optimum control of a floating wave-energy converter with restricted amplitude, J. Offshore Mech. Arct. Eng. 118 (2) (1996) 96–102.

[6] L.V. Perez, G.O. Garcia, State constrained optimal control applied to supervisory control in HEVs, Oil Gas Sci. Technol. – Revue de l'Institut Francais du Petrole 65 (1) (2010) 191–201.

[7] J. Hals, J. Falnes, T. Moan, Constrained optimal control of a heaving buoy wave-energy converter, J. Offshore Mech. Arct. Eng. 133 (1) (2011) 011401.

[8] M.T. Sichani, J.B. Chen, M.M. Kramer, S.R.K. Nielsen, Constrained optimal stochastic control of non-linear wave energy point absorbers, Appl. Ocean Res. 47 (2014) 255–269.

[9] L. Wang, J. Engstrom, M. Goteman, J. Isberg, Constrained optimal control of a point absorber wave energy converter with linear generator, J. Renew. Sustain. Energy 7 (4) (2015) 043127.

[10] W. Cummins, The impulse response functions and ship motions, Schiffstechnik 9 (1962) 101–109.

[11] S.R.K. Nielsen, Z. Zhang, Stochastic Dynamics, Aarhus University Press, 2017.

[12] J. Falnes, Ocean Waves and Oscillating Systems: Linear Interactions Including Wave-Energy Extraction, Cambridge University Press, 2002.

[13] WAMIT, User Manual, Version 7.0, Technical Report, 2011.

[14] S.R.K. Nielsen, Q. Zhou, M.M. Kramer, B. Basu, Z. Zhang, Optimal control of nonlinear wave energy point converters, Ocean Eng. 72 (2013) 176–187.

[15] J.B. Roberts, P.D. Spanos, Random Vibration and Statistical Linearization, Courier Corporation, 2003.

[16] N.E. Huang, et al., The empirical mode decomposition and the Hilbert spectrum for nonlinear and non-stationary time series analysis, Proc. R. Soc. Lond. A: Math. Phys. Eng. Sci. 454 (1998) 903–995.

[17] H. Cramer, M.R. Leadbetter, Stationary and Related Stochastic Processes, Wiley, New York, 1967.

[18] K. Hasselmann, T.P. Barnett, E. Bouws, et al., Measurements of Wind Wave Growth and Swell Decay During the Joint North Sea Project (JONSWAP), Deutches Hydrographisches Institut, 1973.

[19] A.S. El-Bakry, R.A. Tapia, T. Tsuchiya, Y. Zhang, On the formulation and theory of the Newton interior-point method for nonlinear programming, J. Optim. Theory Appl. 89 (3) (1996) 507–541.